XXXVII Brazilian Meeting on Nuclear Physics IOP Publishing
Journal of Physics: Conference Series **630** (2015) 012045 doi:10.1088/1742-6596/630/1/012045

Cold quark matter under intense magnetic fields: the role of flavor mixing and vector interactions

P. G. Allen[a], V. Pagura[b,c] and N. N. Scoccola[a,b,d]

[a] Department of Theoretical Physics, Comisión Nacional de Energía Atómica, Av.Libertador 8250, 1429 Buenos Aires, Argentina
[b]CONICET, Rivadavia 1917, 1033 Buenos Aires, Argentina
[c]IFLP, CONICET − Dpto. de Física, Universidad Nacional de La Plata, C.C. 67, (1900) La Plata, Argentina
[d] Universidad Favaloro, Solís 453, 1078 Buenos Aires, Argentina

Abstract. We study the effect of intense magnetic fields on the phase diagram of cold, strongly interacting matter within the Nambu-Jona-Lasinio model. Model extensions that include flavor mixing effects and vector interactions were analyzed, varying all relevant model parameters in acceptable ranges. Charge neutrality and beta equilibrium effects, which are specially relevant to the study of compact stars, were also considered.

1. Introduction

The influence of intense magnetic fields on the properties of strongly interacting matter has become an issue of increasing interest in recent years [1]. This is mostly motivated by the realization that in some relevant physical situations, like high energy non-central heavy ion collisions [2] and compact stellar objects called magnetars [3], very strong magnetic fields may be produced. Since in these systems extreme temperatures and/or densities may be found, it is interesting to investigate which modifications are induced by the presence of strong magnetic fields on the whole QCD phase diagram. Unfortunately, even in the absence of those fields, the present knowledge of such phase diagram is only schematic due to the well-known difficulty given by the so-called sign problem which affects lattice calculations at finite chemical potential [4]. Of course, the presence of strong magnetic fields makes the situation even more complex. Thus, most of our present knowledge of their effect comes from investigations performed in the framework of effective models (see e.g. [5] and refs. therein). In this contribution we present some results of a study of the phase diagram of cold quark matter subject to intense magnetic fields in the framework of a generalized Nambu-Jona-Lasinio (NJL) model. The NJL-type models are effective relativistic quark models for non perturbative QCD, where gluon degrees of freedom are integrated out and interactions are modelled through point like interactions. In its simplest version [6] it only includes scalar and pseudo scalar interactions that describe chiral symmetry breaking effectively. As well known, however, a more detailed description of the low-energy quark dynamics requires that other channels like flavor mixing and vector meson interactions are taken into account [7]. In fact, some aspects of the effect of those interactions on the magnetized quark matter have already been investigated [8, 9]. The purpose of the present work is to extend those analyses putting special emphasis on the way in which the so-called inverse magnetic catalysis [10] is affected. Moreover, the phase diagram of cold magnetized

quark matter under conditions relevant for the physics of compact stars will be also analyzed. This contribution is organized as follows. In Sec. 2 we provide some details of the model and its parametrizations as well as the way to deal with an external constant magnetic field. In Sec. 3 we present and discuss our results for symmetric quark matter. The situation for stellar matter is analyzed in Sec. 4. Finally, our conclusions are given in Sec. 5.

2. Formalism

We consider the most general SU(2) Lagrangian density which includes a scalar-pseudoscalar interaction, vector-axial vector and the t´Hooft determinant interaction [7]. In the presence of an external magnetic field and chemical potential it reads:

$$\mathcal{L} = \bar{\psi}\left(i \not{D} - m_c + \hat{\mu}\,\gamma^0\right)\psi + \mathcal{L}_{int} \tag{1}$$

where

$$\begin{aligned}\mathcal{L}_{int} &= G_1 \sum_{a=0}^{3}\left[\left(\bar{\psi}\tau_a\psi\right)^2 + \left(\bar{\psi}i\gamma_5\tau_a\psi\right)^2\right] + G_2\sum_{a=0}^{3}\left[\left(\bar{\psi}\gamma_\mu\tau_a\psi\right)^2 + \left(\bar{\psi}\gamma_\mu\gamma_5\tau_a\psi\right)^2\right] \\ &+G_3\left[\left(\bar{\psi}\gamma_\mu\psi\right)^2 + \left(\bar{\psi}\gamma_\mu\gamma_5\psi\right)^2\right] + G_4\left[\left(\bar{\psi}\gamma_\mu\psi\right)^2 - \left(\bar{\psi}\gamma_\mu\gamma_5\psi\right)^2\right] + 2G_D\left(d_+ + d_-\right)\end{aligned} \tag{2}$$

Here, G_i with $i = 1, 4$ and G_D are coupling constants, $\psi = (u, d)^T$ represents a quark field with two flavors, $d_\pm = det\left[\bar{\psi}\left(1 \pm \gamma_5\right)\psi\right]$, $\hat{\mu} = \mathrm{diag}\left(\mu_u, \mu_d\right)$ the quark chemical potentials, m_c is the (current) mass matrix that we take to be the same for both flavors, $\tau_0 = I$, where I is the unit matrix in the two flavor space, and τ_a, $0 < a \leq 3$ denote the Pauli matrices. The coupling of the quarks to the electromagnetic field $\mathcal{A}_\mu$ is implemented through the covariant derivative $D_\mu = \partial_\mu - i\hat{q}\mathcal{A}_\mu$ where $\hat{q}$ represents the quark electric charge matrix $\hat{q} = \mathrm{diag}\left(q_u, q_d\right)$ where $q_u/2 = -q_d = e/3$. In the present work we consider a static and constant magnetic field in the 3-direction, $\mathcal{A}_\mu = \delta_{\mu 2}x_1 B$. In the mean-field approximation the associated grand-canonical thermodynamical potential for cold and dense quark matter reads

$$\Omega^{\mathrm{MFA}} = -\sum_{f=u,d}\theta_f + \Omega_{pot} \tag{3}$$

where θ_f gives the contribution from the gas of quasi-particles of each flavor $f = u, d$ and can be written as the sum of 3 contributions [11]

$$\begin{aligned}\theta_f^{\mathrm{vac}} &= \frac{N_c}{8\pi^2}\left\{\Lambda\left(2\Lambda^2 + M_f^2\right)\sqrt{\Lambda^2 + M_f^2} - M_f^4\ln\left[\frac{(\Lambda + \sqrt{\Lambda^2 + M_f^2})}{M_f}\right]\right\}, \\ \theta_f^{\mathrm{mag}} &= \frac{N_c}{2\pi^2}\left(|q_f|B\right)^2\left[\zeta^{(1,0)}(-1, x_f) - \frac{1}{2}(x_f^2 - x_f)\ln x_f + \frac{x_f^2}{4}\right], \\ \theta_f^{\mathrm{med}} &= \frac{N_c}{4\pi^2}\,|q_f|B\sum_{\nu=0}^{\nu_f^{max}}\alpha_\nu\left[\tilde{\mu}_f\sqrt{\tilde{\mu}_f^2 - s_f(\nu, B)^2}\right. \\ &\qquad\left. -s_f(\nu, B)^2\ln\left(\frac{\tilde{\mu}_f + \sqrt{\tilde{\mu}_f^2 - s_f(\nu, B)^2}}{s_f(\nu, B)}\right)\right],\end{aligned} \tag{4}$$

where $M_f = m_c + \sigma_f$ and $\tilde{\mu}_f = \mu_f - \omega_f$, with σ_f and ω_f being the mean field values of the scalar and vector meson fields, respectively. Λ represents a non covariant ultraviolet cutoff and

$\zeta^{(1,0)}(-1,x_f) = d\zeta(z,x_f)/dz|_{z=-1}$ where $\zeta(z,x_f)$ is the Riemann-Hurwitz zeta function. In addition, $s_f(\nu,B) = \sqrt{M_f^2 + 2|q_f|B\nu}$ while $x_f = M_f^2/(2|q_f|B)$. In θ_f^{med}, the sum is over the Landau levels (LLs), represented by ν, while $\alpha_\nu = 2 - \delta_{\nu 0}$ is a degeneracy factor and ν_f^{max} is the largest integer that satisfies $\nu_f^{max} \leq (\tilde{\mu}_f^2 - M_f^2)/(2|q_f|B)$.

The Ω_{pot} contribution reads

$$\Omega_{pot} = \frac{(1-c_s)(\sigma_u^2+\sigma_d^2) - 2c_s\,\sigma_u\,\sigma_d}{8g_s(1-2c_s)} - \frac{(1-2c_v)(\omega_u^2+\omega_d^2) + c_v\,\omega_u\,\omega_d}{8g_v(1-2c_v)} \tag{5}$$

where we have introduced a convenient parametrization of the coupling constants in terms of the quantities g_s, c_s, g_v and c_v given by

$$\begin{aligned} g_s &= G_1 + G_D \quad ; \quad g_v = G_2 + G_3 + G_4 \\ c_s &= \frac{G_D}{G_1+G_D} \quad ; \quad c_v = \frac{G_3+G_4}{2(G_2+G_3+G_4)} \end{aligned} \tag{6}$$

The relevant gap equations are given by

$$\frac{\partial\Omega^{\rm MFA}(\sigma_u,\sigma_d,\omega_u,\omega_d)}{\partial(\sigma_u,\sigma_d,\omega_u,\omega_d)} = 0\ . \tag{7}$$

In our calculations we will consider first the simpler case of symmetric matter where both quarks carry the same chemical potential μ. Afterwards, we will analyze the case of stellar matter in which leptons are also present and β-equilibrium and charge neutrality are imposed. In this case the chemical potential for each quark, μ_f, is a function of μ and the lepton chemical potentials which have to be selfconsistently determined.

In order to analyze the dependence of the results on the model parameters, we will consider two SU(2) NJL model parametrizations. Set 1 corresponds to that leading to $M_0 = 340$ MeV while Set 2 to that leading to $M_0 = 400$ MeV. Here, M_0 represents the vacuum quark effective mass in the absence of external magnetic fields. The corresponding model parameters are listed in Table 1.

Table 1. Parameter sets for the NJL SU(2) model.

Parameter set	M_0 MeV	m MeV	$g_s\Lambda^2$	Λ MeV	$-<u\bar{u}>^{1/3}$ MeV
Set 1	340	5.595	2.212	620.9	244.3
Set 2	400	5.833	2.440	587.9	240.9

The presence of the t'Hooft determinant interaction is very important since it reflects the $U_A(1)-$anomaly of QCD. Its strength, and consequently the amount of flavor mixing induced by this term, is controlled by the parameter c_s. An estimate for its value can be obtained from the $\eta - \eta'$ mass splitting within the 3−flavor NJL model [12]. This leads to $c_s \simeq 0.2$ [13]. In any case, to obtain a full understanding of the effects of flavor mixing we will vary the value of c_s in a range going from 0, which corresponds to a situation in which the two flavors are completely decoupled, to 0.5, being this the case of maximum flavor mixing described for example in Ref. [14]. Regarding the vector term coupling g_v it is important to recall that one can obtain naturally the vector axial-vector interaction if one starts from a QCD-inspired color current-current interaction and then performs a Fierz transform into color-singlet channels, and

that in this case the relation between coupling strengths is $g_v = g_s/2$ [7]. Yet, the value of g_v cannot be accurately determined from experiments nor from lattice QCD simulations and this is why it has been taken as a free parameter in most works. In the present work we take $0 < g_v/g_s < 0.5$. It is worth mentioning that due to the mixing of pseudoscalar and longitudinal axial vector interaction terms pseudoscalar meson properties depend on g_v. Thus, strictly speaking the parameters given in Table 1 only lead to the empirical values of f_π and m_π when $g_v = 0$. However, as shown in Ref. [15], m_π and f_π only change by $\sim 10\%$ when g_v/g_s increases from 0 to 1. Thus, for simplicity, we will keep the model parameter values fixed when varying g_v. A last comment regarding c_v, i.e. the parameter that regulates the ratio between the singlet and octet vector-axial vector interaction strengths: we will take it as a free parameter in the range $0 \leq c_v \leq 1/2$. Note that for $c_v = 1/2$ only singlet vector-axial interactions are present and, thus, there is no mixing between the pseudoscalar and longitudinal axial vector channels.

We end this section by describing the way in which the different phases of the magnetized quark matter will be denoted as well as the procedure used to identify the boundaries between them. For the phases we adopt the notation of Refs. [14, 16]. Thus, the vacuum (i.e. fully chirally broken) phase is denoted by B, the massive phases in which M_f depends on the chemical potential by C_α and, finally, the chirally restored phases by A_α. Here, α is a set of two numbers indicating the highest LL populated for each flavor. To obtain the critical chemical potential at a given eB we proceed as follows. In the case of first order phase transitions we calculate the thermodynamical potential for each of the neighboring phases and then searched the chemical potential at which these values become degenerate. In the case of crossover transitions the critical value is identified by the peak of the chiral susceptibility corresponding to each quark flavor.

3. Results for symmetric matter

In this section we present the results obtained for the case of symmetric matter. These results were obtained solving the set of coupled "gap equations", Eqs. (7), for different values of magnetic field and chemical potential. In order to understand the effect of the different terms in the Lagrangian we consider in Sec. 3.1 the effect of flavor mixing on quark behavior within the model in the absence of vector interactions. The role of those interactions will be subsequently addressed in Sec. 3.2.

3.1. Effect of the flavor mixing interactions

To neglect vector interactions implies taking $G_2 = G_3 = G_4 = 0$ in Eq. (2), while $G_1 \neq 0$ and $G_D \neq 0$. Therefore, Eqs. (7), will become a set of two coupled equations that must be solved for the independent variables M_u and M_d. The parameter c_s acts as a coupling between both flavors and we study how the phase transitions are modified as we vary this parameter in the range $0 \leq c_s \leq 0.5$.

The case $c_s = 0.5$ corresponds to ordinary NJL where flavor mixing is maximum and, thus, both flavors have identical behavior. In fact, the first term in Eq. (5) will tend to infinity as c_s goes to 0.5 unless $M_u = M_d$, which leaves only one equation to be solved. But if $c_s < 0.5$, then both masses will be independent variables, and transitions for each flavor might occur simultaneously or not in different regions of the phase diagrams.

It is common to all these cases that chiral symmetry is completely broken for chemical potentials well below M_0 and that restoration occurs for high enough chemical potentials, usually accompanied by a large drop in the dressed mass. The inclusion of a constant magnetic field modifies the quark dispersion relations, introducing Landau levels (LL's) into its spectrum. A consequence of this is that chiral symmetry restoration occurs in several steps, each of which is a transition where quark population appears on previously unoccupied LL's. This gives rise to a potentially complex phase diagram, whose precise form depends on the parameter set and

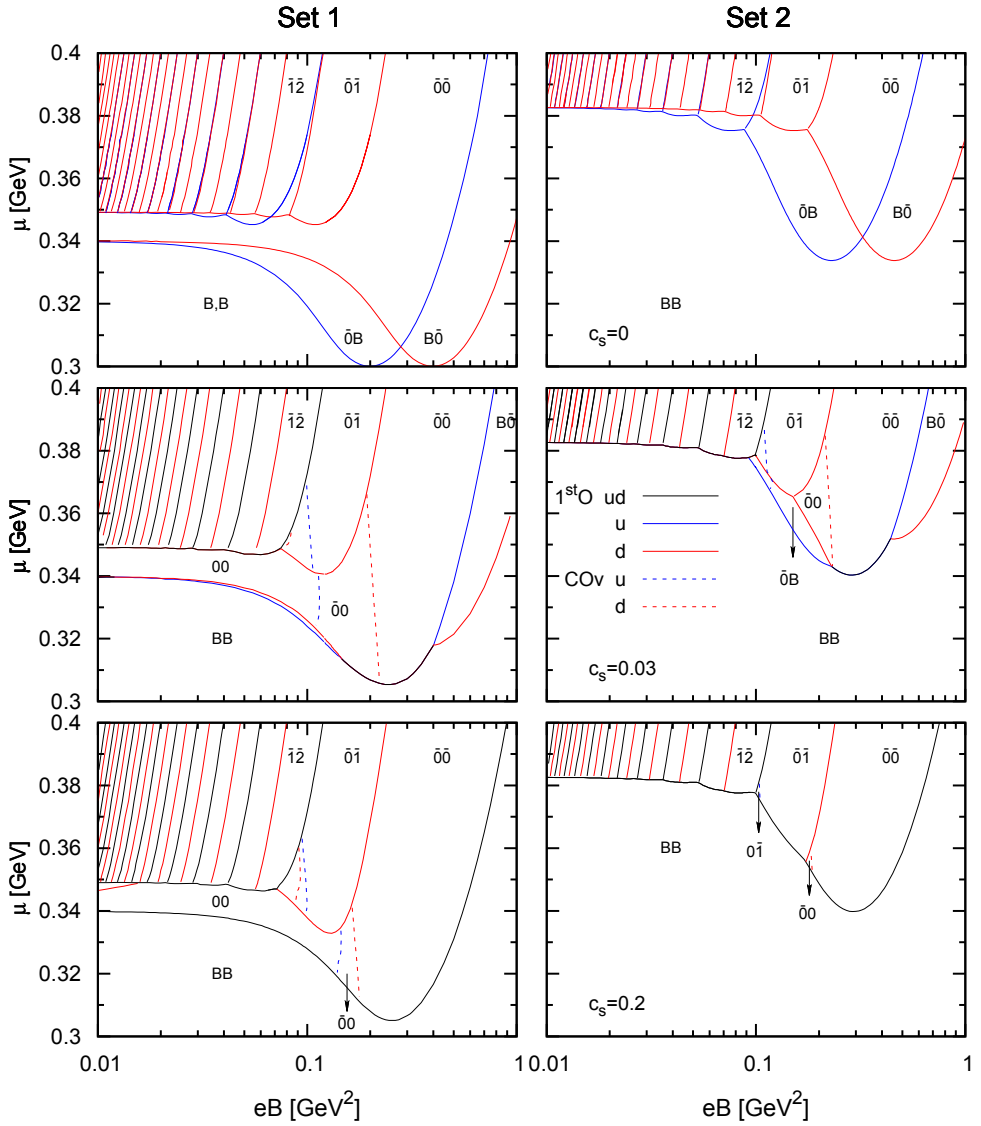

Figure 1. (Color online) Phase diagrams in the $eB - \mu$ plane for different values of flavor-mixing parameter c_s. To simplify the figure we have introduced a compact notation to indicate the phases. The pair of integers mn corresponds to the C_{mn} phase and the pair $\bar{m}\bar{n}$ to the A_{mn} phase. The case in which one quark is in a C-type phase and the other in the A-type phase is indicated by putting a bar on top of the integer associated with the A-type phase.

magnetic field (The $B = 0$ case is simple yet depending on the parameter set there can be a few differences).

We will start by analyzing the phase transitions for the case with no flavor mixing, i.e. $c_s = 0$, previously studied in Ref. [8]. The phase diagrams for both parameter sets can be seen in the upper two panels of Fig. 1. In a sense, each flavor will have its own independent phase diagram because the gap equations are decoupled. Here, each line corresponds to a transition where LL population of a single quark flavor occurs (red lines for down quarks, blue lines for up quarks). Both flavors will coincide for $B = 0$ where $SU(2)$ symmetry is recovered and behave differently as B increases, due to their different electric charges. Since this is the only difference between

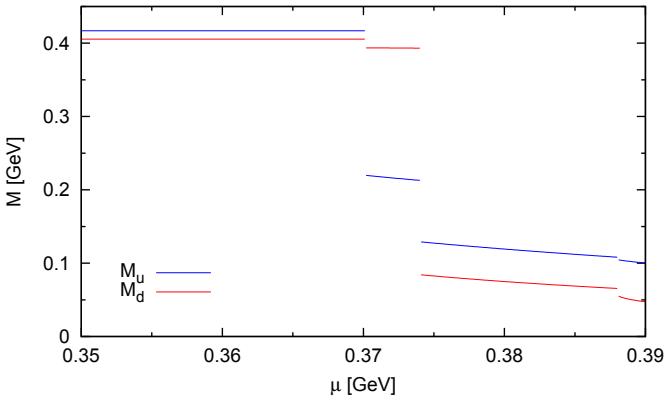

Figure 2. (Color online) Dressed masses for both flavors for Set 2, $c_s = 0.03$, for $eB = 0.11$ GeV^2.

the equations for both flavors and since it only appears in the product $q_f B$, one phase diagram may be obtained from the other one through the replacement $q_u B = (2q_d)B = q_d(2B)$ which amounts to a stretching along the B axis of its phase diagram with respect to the up quark one.

When c_s becomes finite (second row onwards in Fig. 1), flavors become coupled and a complex pattern is created, where transitions move closer together in some regions and even merge together in others, that is, the LL population changes simultaneously for both flavors (these are represented by black lines). We can see that already for $c_s = 0.03$, the transitions in both parameter sets occur together for low magnetic fields, and then separate for $B = 0.02$ GeV^2 (in Set 1) and $B = 0.1$ GeV^2 in Set 2.

In order to make the meaning of the transition lines clearer, we present on Fig. 2 the dressed masses for both flavors for Set 2, $c_s = 0.03$, for $eB = 0.11$ GeV^2. When the first discontinuity is encountered, at $\mu = 370$ MeV, M_u jumps to half its value and its lowest LL (LLL) becomes populated. On the other hand, the down flavor remains in vacuum. Actually, its mass presents a small discontinuity caused by the weak coupling to the up quark which is not to be interpreted as a down transition. The down quark LLL is occupied at $\mu = 374$ MeV. When both flavors are in the vacuum phase, $M_u > M_d$, while in the populated phase it happens the other way around, which is consistent with the phenomena of catalysis and anticatalysis discussed in Ref. [14].

For $c_s = 0.2$, the transitions for both flavors occur together, so the qualitative behavior is very similar to the full flavor mixing case $c_s = 0.5$. In fact, the model tends to full mixing quite quickly and only for $c_s \lesssim 0.1$ are relevant mixture effects (or more precisely, the absence of it) actually seen. On the other hand, cross over transitions do not have this property and tend much more slowly to the $c_s = 0.5$ behavior.

3.2. Effect of the vector interactions

In this section we analyze the effect of vector interaction terms. As discussed in the previous section, for $c_s \gtrsim 0.1$ the phase diagrams do not present qualitative variations. Here, therefore, we consider $c_s = 0.2$ which also is in the range of realistic values suggested in Ref. [13]. Although these results correspond to $c_v = 0$, our studies show that only small quantitative differences occur when varying this parameter from 0 to 1.

In Fig. 3 we present a series of phase diagrams obtained for different values of the ratio g_v/g_s. The left column corresponds to Set 1 while the right column was obtained with parameter Set 2.

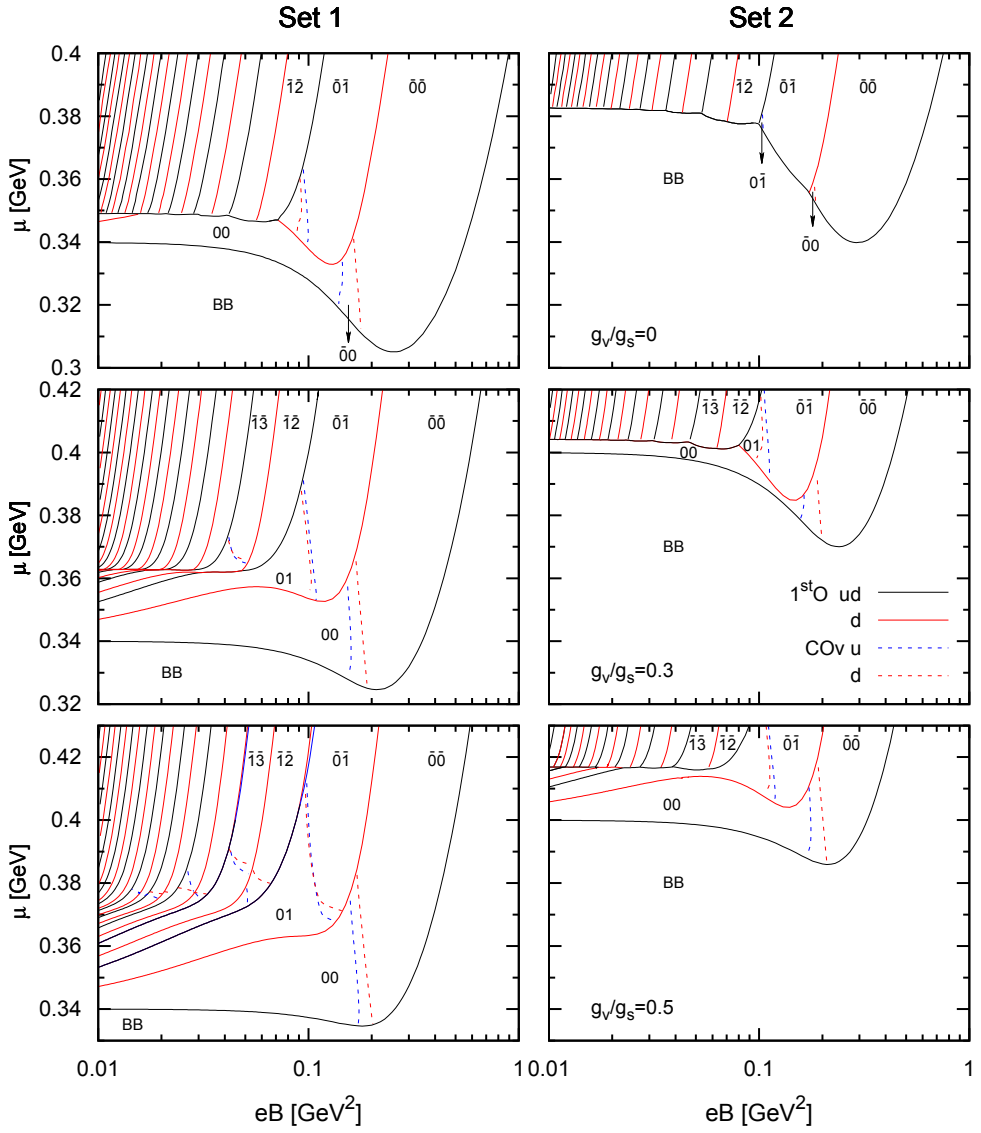

Figure 3. (Color Online) Phase diagrams in the $eB - \mu$ plane for different values of g_v/g_s. Different phases are denoted as in Fig. 1

For Set 1 we observe that as g_v/g_s increases the two lower and main transitions separate and several new transitions appear in the low eB region of the diagram. For Set 2 at some small $g_v/g_s \simeq 0.1$ the lower transition first splits into two, leaving a 00 phase in between which was not present before. For larger values of g_v/g_s the behavior is similar to that of Set 1. The appearance of new transitions at low eB as g_v/g_s increases is clearly seen in the left panel of Fig. 4, where we show d quark density normalized to nuclear matter density ($\rho_0 = 1.30$ MeV^3) as a function of chemical potential for $eB = 0.016$ GeV in Set 1. In the absence of vector interaction, the density jumps from close to 0 to 3 times nuclear matter density, while quark population jumps from 00 to high LLs occupied. As g_v increases, the amount of transitions increases too. In fact, increasing the vector interaction coupling has the same effect as going to a parameter set that reproduces a lower value of current mass M_0, described in Ref. [14]. Notice that the phase diagram for Set 2 and $g_v/g_s = 0.3$ is in this sense very similar to Set 1 and $g_v/g_s = 0$.

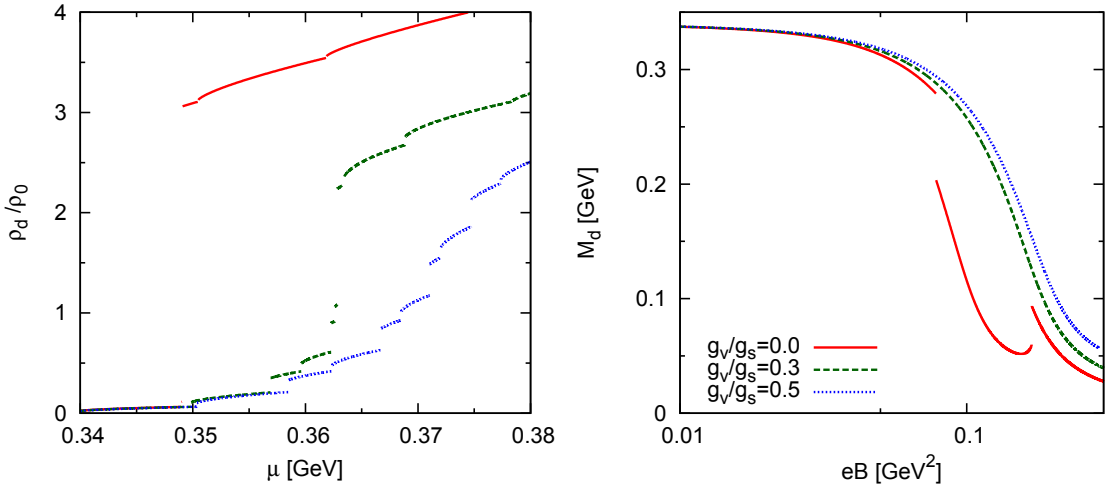

Figure 4. (Color online) Quark density over nuclear matter density as function of the chemical potential for $eB = 0.016$ GeV^2 (left) and current mass as function of magnetic field for $\mu = 0.345$ GeV (right) for different values of g_v/g_s. Results correspond to d flavor and were obtained with parameter Set 1.

It was also found that as vector coupling is increased, the inverse magnetic catalysis effect becomes attenuated. This can be observed in the right panel of Fig. 4 where we plot the current quark mass for d quarks as a function of the magnetic field for $\mu = 345$ MeV, for all g_v/g_s values considered here. For low magnetic fields, the mass remains constant and after $eB \sim 0.02$ GeV^2 it starts to decrease smoothly. This decrease, however, is less abrupt for higher g_v values. The first discontinuity found in the current mass for $g_v/g_s = 0$ correlates to the d quark transition from the phase 00 to 01. For a higher eB there is a second discontinuity, in this case a jump to a higher mass value, corresponding to a return to phase 00. Moreover, if we measure the depth of the IMC "well" as the difference in μ between the lowest critical chemical potential at $eB = 0$ MeV and the lowest possible one in the whole diagram, we find that this $\Delta\mu$ is reduced by an 84% for Set 1 and by a 67% for Set 2 when going from $g_v = 0$ to $g_v = 0.5$.

4. Results for stellar matter

We now turn our attention to stellar matter. Following the discussions in the previous section only results for $c_s = 0.2$ will be presented. If charge neutrality is imposed on our system, there will be a fixed relation between the densities of the up and down quarks, which will be necessarily different unless they are both zero. So, even though the value of $c_s = 0.2$ was close enough to the full mixing case according to what was established in previous sections, charge neutrality will cause the flavors to behave differently among themselves.

The phase diagrams in the $\mu - B$ plane for both parameter sets and for increasing values of g_v are plotted in Fig. 5. The chemical potential μ on the horizontal axis is now the quark number chemical potential, which is related to flavor chemical potentials through $\mu = \mu_u + 2\mu_e/3$ and $\mu = \mu_d - \mu_e/3$. The introduction of charge neutrality has a few effects similar to those of vector interaction, in the sense that diagrams become similar to the ones corresponding to lower M_0 sets: main transitions separate for low eB and several transitions appear in the region between them. The magnetic anticatalysis effect is reduced also: The depth of the anticatalysis well, as defined in the previous section, is reduced from 35 MeV to 9 MeV in Set 1 and from 43 MeV to 22 MeV in Set 2. As expected, the introduction of vector interaction will further enhance these effects, so that anticatalysis has completely disappeared for $g_v = 0.5$.

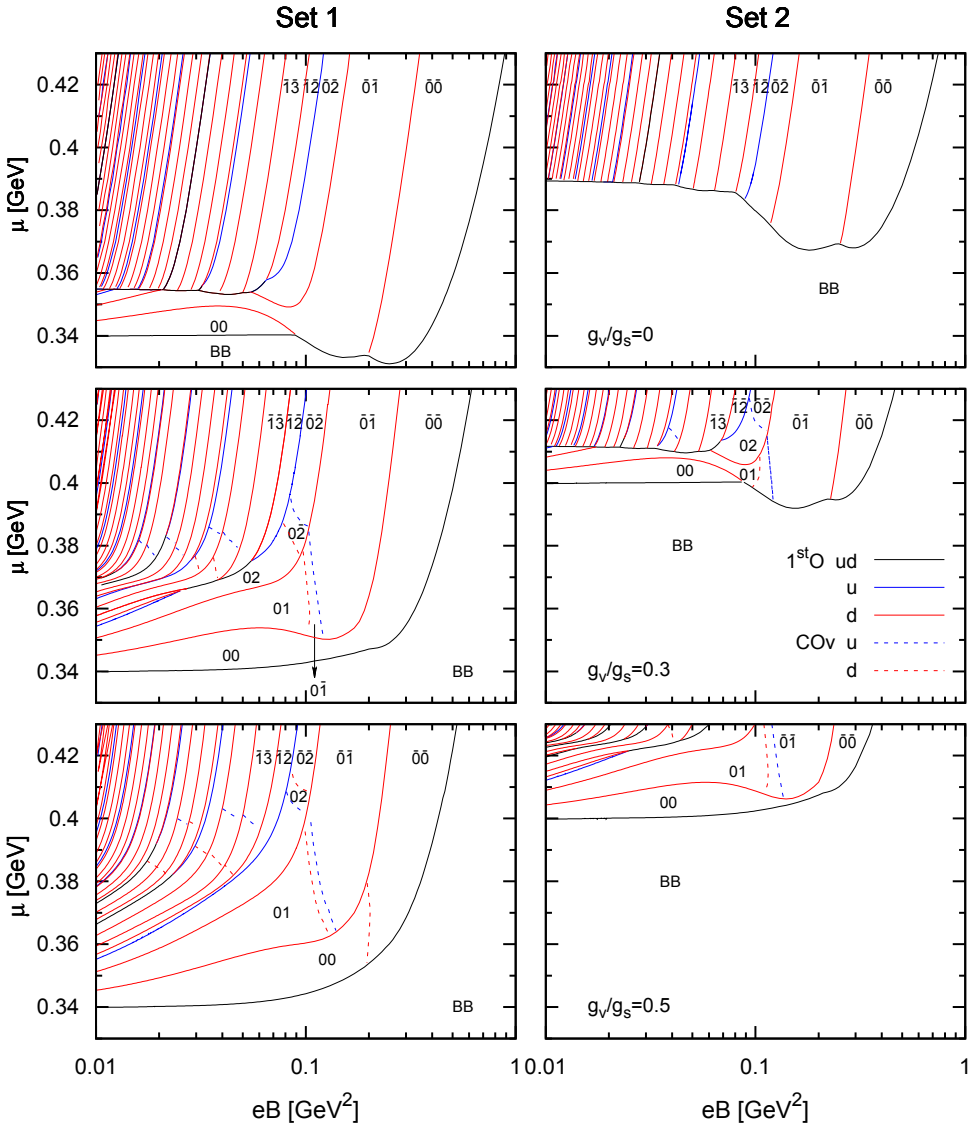

Figure 5. (Color online) Phase diagrams in the $eB - \mu$ plane for stellar matter and different values of g_v/g_s. Different phases are denoted as in Fig. 1

The "Van Alphen - de Haas" (VA-dH) transitions acquire relatively independent behaviors when charge neutrality is introduced. In particular, for intermediate $eB\,(\simeq 0.1\ \mathrm{GeV}^2)$ the transition between $k_u = 0$ and $k_u = 1$ is well separated from the down transition. For symmetric matter, the VA-dH transitions occurred to a very good level of approximation for a critical chemical potential $\mu_c = \sqrt{2kq_fB}$ (being this condition exact for the chiral case), so the relation between the charges produced one up transition every two down transitions. Although this relation is still satisfied for each flavor chemical potential, these are now different between themselves and related through $\mu_u\ -\mu_d\ +\mu_e = 0$. As a result of this, in Fig. 5 we roughly have one up transition every four down transitions.

5. Conclusions

We have investigated how the phase diagram of cold strongly interacting matter is modified in the presence of intense magnetic fields in the context of NJL-type models which include flavor mixing and vector interaction. The whole range of possible flavor mixing values was swept through. For symmetric matter it was found that for rather small values of the flavor mixing parameter, $c_s = 0.1$, phase diagrams already display a behavior that is qualitatively very similar to the full mixing case. The role of the vector interactions and stellar matter conditions were studied for $c_s = 0.2$, which is deduced from $SU(3)$ estimates. The relevant effects are similar to those occurring when changing to a parameter set that fits to a smaller dressed mass. Particularly interesting is the reduction of the Inverse Magnetic Catalysis phenomenon, which can completely disappear by the joint effect of the vector interactions and the stellar matter conditions.

Acknowledgments

This work was partially supported by CONICET (Argentina) under grant PIP 00682 and by ANPCyT (Argentina) under grant PICT-2011-0113.

References

[1] D.E. Kharzeev, K. Landsteiner, A. Schmitt and H.-U. Yee, Lect. Notes Phys. 871 (2013) 1.
[2] D.E. Kharzeev, L.D. McLerran and H.J. Warringa, Nucl. Phys. A803 (2008) 227.
[3] R.C. Duncan and C. Thompson, Astrophys J. 392 (1992) L9.
[4] F. Karsch, E. Laermann, 2004 *Quark Gluon Plasma 3*, edited by R.C.Hwa et al. (World Scientific Singapore), p.1.
[5] E.S. Fraga, Lect. Notes Phys. 871 (2013) 121; R. Gatto and M. Ruggieri, Lect. Notes Phys. 871 (2013) 87.
[6] Y. Nambu and G. Jona-Lasinio, Phys. Rev. **122** (1961) 345; **124** (1961) 246.
[7] U. Vogl and W. Weise, Prog. Part. Nucl. Phys. **27** (1991) 195; S. Klevansky, Rev. Mod. Phys. **64** (1992) 649; T. Hatsuda and T. Kunihiro, Phys. Rep. **247** 221 (1994) 221.
[8] J. K. Boomsma and D. Boer, Phys. Rev. D **81** (2010) 074005.
[9] R. Z. Denke and M. B. Pinto, Phys. Rev. D **88** (2013) 056008; D. P. Menezes, M. B. Pinto, L. B. Castro, P. Costa and C. Providência, Phys. Rev. C **89** (2014) 055207.
[10] F. Preis, A. Rebhan and A. Schmitt, JHEP **1103** (2011) 033; F. Preis, A. Rebhan and A. Schmitt, Lect. Notes Phys. **871** (2013) 51.
[11] D.P. Menezes, M.B. Pinto, S.S. Avancini, A. Pérez Martínez and C. Providência, Phys. Rev. **C 79** (2009) 035807; D.P. Menezes, M.B. Pinto, S.S. Avancini and C. Providência, Phys. Rev. **C 80** (2009) 065805; S.S. Avancini, D.P. Menezes and C. Providência, Phys. Rev. **C 83** (2011) 065805.
[12] T. Kunihiro, Phys. Lett. B **219** (1989) 363 [Erratum-ibid. B **245** (1990) 687].
[13] M. Frank, M. Buballa and M. Oertel, Phys. Lett. B **562** (2003) 221.
[14] P. G. Allen and N. N. Scoccola, Phys. Rev. D **88** (2013) 094005.
[15] M. Hanauske, L. M. Satarov, I. N. Mishustin, H. Stoecker and W. Greiner, Phys. Rev. D **64** (2001) 043005.
[16] D. Ebert, K. G. Klimenko, M. A. Vdovichenko, and A. S. Vshivtsev, Phys. Rev. D **61** (1999) 025005.